UNIVERSITÀ DEGLI STUDI DI TORINO

1 **Title**: Positive-charged solid lipid nanoparticles as paclitaxel drug delivery system in glioblastoma

2 treatment.

3 **Author names and affiliations**: Daniela Chirio[a], Marina Gallarate[a], Elena Peira[a], Luigi Battaglia[a],

4 Elisabetta Muntoni[a], Chiara Riganti[b], Elena Biasibetti[c], Maria Teresa Capucchio[c], Alberto Valazza[c],

5 Pierpaolo Panciani[d], Michele Lanotte[d], Laura Annovazzi[e], Valentina Caldera[e], Marta Mellai[e],

6 Gaetano Filice[f], Silvia Corona[f], Davide Schiffer[e]

7 [a] University of Turin, Dipartimento di Scienza e Tecnologia del Farmaco, via Giuria 9, 10125

8 Torino, Italy.

9 daniela.chirio@unito.it, marina.gallarate@unito.it, elena.peira@unito.it, luigi.battaglia@unito.it,

10 elisabetta.muntoni@unito.it

11 [b] University of Turin, Dipartimento di Oncologia, Regione Gonzole 10, 10043 Orbassano (TO),

12 Italy.

13 chiara.riganti@unito.it

14 [c] University of Turin, Dipartimento di Scienze Veterinarie, Largo Paolo Braccini 2, 10095

15 Grugliasco (TO), Italy.

16 elena.biasibetti@unito.it, mariateresa.capucchio@unito.it, alberto.valazza@unito.it

17 [d] University of Turin, Dipartimento di Neuroscienze, Via Cherasco 15, 10126 Torino, Italy.

18 vincy.bip@alice.it, michele.lanotte@unito.it

19 [e] Policlinico di Monza, Centro di NeuroBioOncologia, Via Pietro Micca 29, 13100 Vercelli, Italy.

20 davide.schiffer@unito.it, laura.annovazzi@cnbo.it, valentina.caldera@cnbo.it,

21 marta.mellai@cnbo.it

22 [f] IRCCS Policlinico San Matteo, University of Pavia, Dipartimento di Malattie Infettive, V.le Golgi

23 19, 27100 Pavia, Italy,

24 gaetano.filice@unipv.it

25

26

Corresponding Author: Daniela Chirio, via P. Giuria 9, 10125 Torino, Italy

daniela.chirio@unito.it

Phone: +39 0116707668   Fax: +39 0116707687

Abstract

Paclitaxel loaded solid lipid nanoparticles (SLN) of behenic acid were prepared with the coacervation technique. Generally, spherical shaped SLN with mean diameters in the range 300-600 nm were obtained. The introduction of charged molecules, such as stearylamine and glycol chitosan into the formulation allowed to obtain positive SLN with Zeta potential in the 8-20 mV range and encapsulation efficiency in the 25-90% range.

Blood-brain barrier (BBB) permeability, tested in vitro through hCMEC/D3 cells monolayer, showed a significantly increase in the permeation of Coumarin-6, used as model drug, when vehicled in SLN. Positive-charged SLN do not seem to enhance permeation although stearylamine-positive SLN resulted the best permeable formulation after 24 h.

Cytotoxicity studies on NO3 glioblastoma cell line demonstrated the maintenance of cytotoxic activity of all paclitaxel-loaded SLN that was always unmodified or greater compared with free drug. No difference in cytotoxicity was noted between neutral and charged SLN.

Co-culture experiments with hCMEC/D3 and different glioblastoma cells evidenced that, when delivered in SLN, paclitaxel increased its cytotoxicity towards glioblastoma cells.

Abbreviations:

PTX, paclitaxel; SLN, solid lipid nanoparticles; BA, behenic acid; ST, stearylamine; GCS, glycol chitosan; BBB, blood-brain barrier; GBM, blioblastoma multiforme; CNS, central nervous system; NP, nanoparticles; cationic bovine serum albumin, CBSA; NHEJ, non-homologous end joining; PK, protein Kinase; CS, chitosan; Cou-6, coumarin 6; Na-BA, sodium behenate; CHOL, cholesterol; FD, freeze-dried; DMEM, Dulbecco's modified Eagle's medium; NS, neurosphere;

AC, adherent cell; ATM, ataxia telangiectasia mutated; ChK2, checkpoint kinase; p-53BP1, 53

binding protein 1; MTT, 3-(4,5-dimethylthiazol-2-yl)-2,5diphenyl-tetrazolium bromide; IF,

immunofluorescence; HR, homologous recombination; TEM, transmission electron microscopy;

EE, entrapment efficiency; Pgp, P-glycoprotein; MRP1, multidrug resistance related protein 1.

Chemical compounds studied in this article:

Paclitaxel (PubChem CID: 36314)

Coumarin-6 (PubChem CID: 100334)

Behenic acid (PubChem CID: 8215)

1. Introduction

Glioblastoma multiforme (GBM) is the most common form of primary brain tumor in the central nervous system (CNS); its aggressive nature and evasiveness to treatments make it one of the most lethal cancers [1]. Current treatments for GBM provide a tumor surgical resection followed by pharmacotherapy and radiotherapy. Pharmacotherapy, directed by residual tumor cells elimination, ranges from common chemotherapeutic agents such as temozolomide to more recent anti-angiogenic agents and immunotherapeutic treatments [2]. However, anti-cancer therapeutic agents have not significantly increased the median survival of GBM patients over the past 10 years. The 5-year survival rate of GBM patients after treatment that includes surgical resection, radiation and chemotherapy, is 9.8%.

The failure of chemotherapy is due to the inability of intravenously administered anticancer agents to reach the brain parenchyma. An endothelial cell monolayer associated with pericytes and astrocytes, known as the blood–brain barrier (BBB), separates blood from the cerebral parenchyma and prevents the penetration of drugs into the CNS.

BBB is a functional unit composed by the peculiar endothelium of brain microvessels, the capillary basal lamina and the surrounding astrocytes, neurons, microglial cells and pericytes, which contribute to the maintenance of the barrier properties [3, Figure A.1]. The presence of tight junctions and adherent junctions between adjacent endothelial cells [4], the lack of fenestrations and pinocytotic vesicles [5], the abundance of efflux transporters belonging to the ATP binding cassette family on the endothelium luminal side [6] account for the low delivery of drugs, such as antineoplastic agents [7], from the bloodstream to the brain parenchima.

Various invasive strategies have been developed to improve the penetration of drugs into the brain [8]. Traditional approach to overcome brain drug delivery obstacles includes direct intracerebral drug injection [9],which is associated with a high risk for the patient.

Less invasive strategies have also been investigated. One approach consists in generating a transient disruption of BBB in conjunction with the systemic administration of anticancer agents. The

4

90   intracarotid administration of a hyperosmotic solution such as mannitol led to a rapid diffusion of

91   fluid across the cerebral endothelium, moving out of the endothelial cells into the vascular lumen

92   and inducing the opening of the tight junctions for a few hours [10].

93   Another approach concerns the modification of drugs in order to make them more lipophilic,

94   improving their penetration into the brain by passive diffusion. Lipophilic analogs and prodrugs

95   were thus developed [11].

96   A more recent strategy to deliver drugs to the brain is the use of colloidal polymers to form

97   nanometer sized carriers [12]. The basic reason of common acceptance of these vehicles is due to

98   their drug release controlled profile of as well as to their selected targeting mechanism. Targeting

99   action may be due to the steric hindrance created by nano-vectors: after parenteral administration,

100   due to steric phenomenon they conceal themselves from opsonization event induced by tissue

101   macrophages. By this way they achieve targeting ability to the brain and partially avoid other

102   reticuloendothelial system organs like liver, spleen, etc [13].

103   From the last few decades, nanoparticles (NP) have attracted considerable interest in targeting drug

104   molecules to the brain [14]. The correct mechanism of barrier opening by NP is not exactly known;

105   the delivered NP enter into the brain by crossing the BBB by various endocytotic mechanisms, as

106   polymeric albumin or poly(butylcyanoacrylate) NP are reported to enter into the brain by their small

107   size mediated endocytosis [15,16]. An increased drug retention in brain blood capillaries combined

108   with an adsorption to capillary can increase drug transport due to an enhanced concentration

109   gradient; an increase of BBB fluidization, an opening of tight junctions between endothelial, an

110   inhibition of the P-glycoprotein efflux system are other possible mechanisms that can increase brain

111   drug concentration [17].

112   Although NP may be designed to entrap high molecular weight or hydrophilic therapeutics, BBB

113   retardation of drug NP entrapped is based on NP characteristics and not on the therapeutic agent

114   [18].

Indeed, poly(butyl cyanoacrylate) NP overcoated with 1% polysorbate 80 have been experimentally successful as brain drug delivery for doxorubicin [19] and dalargin [20], poly(lactic-co-glycolic acid) and cetyl alcohol/polysorbate NP for paclitaxel brain delivery [21,22].

In addition to BBB functional characteristics limiting permeation, brain microvasculature endothelia also present a luminal electrostatic barrier at physiologic pH. The negative electrostatic charge is created by surface expression and adhesion of the glycocalyx residues: proteoglycans, sulfated mucopolysaccharides, and sulfated and sialic acid-containing glycoproteins and glycolipids [23]. Cationic molecules have been shown to occupy anionic areas at the BBB endothelium [24] and increase BBB permeability via a presumed tight junction disruption [25].

Recent *in vitro* reports have demonstrated that positive-charged NP have an increased brain distribution compared to anionic and neutral NP [26]. However, there is little data regarding brain permeability of positive-charged NP. Lu et al. [27] developed and evaluated cationic bovine serum albumin (CBSA) conjugated with poly(ethyleneglycol)–poly(lactide) NP (CBSA–NP). To evaluate the effects of brain delivery, BSA conjugated with pegylated NP (BSA–NP) was used as the control group and Coumarin-6 was incorporated into the NP as the fluorescent probe. The qualitative and quantitative results of CBSA–NP uptake experiment compared with those of BSA–NP showed that rat brain capillary endothelial cells took in much more CBSA–NP than BSA–NP at 37 °C, at different concentrations and time incubations. After a dose of 60 mg/kg CBSA–NP or BSA–NP injection in mice caudal vein, fluorescent microscopy of brain coronal sections showed a higher accumulation of CBSA–NP in the lateral ventricle, third ventricle and periventricular region than that of BSA–NP. In an experimental work Lockman et al. [15] evaluated the effect of neutral, anionic and cationic charged NP on BBB integrity and NP brain permeability. Neutral NP and low concentrations of anionic NP had no effect on BBB integrity, whereas, high concentrations of anionic NP and cationic NP disrupted the BBB. The brain uptake rates of anionic NP at lower concentrations were higher than of neutral or cationic formulations at the same concentrations.

In literature, many authors studied solid lipid nanoparticles (SLN) as drug delivery systems to deliver drugs to the CNS [28,29]. SLN are disperse systems having size ranging from 1 to 1000 nm which represent an alternative to polymeric particulate carriers and are composed of physiological or biocompatible lipids or lipid molecules with a history of safe use in therapy and are generally suitable for intravenous administration.

As few data are present in literature about positive-charged SLN for brain delivery, the purpose of this work will be to prepare, characterize and evaluate in vitro the potential of positive-charged SLN to vehicle paclitaxel (PTX) to the brain for GBM treatment.

PTX, a diterpene isolated from *Taxus brevifolia*, is one of the most active chemotherapeutic agents against a wide panel of solid tumors including urothelial, breast, lung, and ovarian cancers. It has been demonstrated that PTX is effective against glioblastoma cells *in vitro* [30,31], however its clinical use is limited due to its poor BBB penetration capability and drug-resistance [32,33].

Due to its low water solubility, PTX is formulated in a mixture of Cremophor® EL and dehydrated ethanol (50:50 v/v) a combination known as Taxol®. However, Taxol® has some severe side effects related to Cremophor® EL and ethanol [34]. Therefore, there is an urgent need for the development of alternative PTX formulations.

Recently, a new solvent-free technique, defined as "coacervation", was developed to prepare fatty acids-based SLN [35]. Briefly, a fatty acid alkaline salt micellar solution in the presence of an appropriate polymeric stabilizer was prepared; when the pH is lowered by acidification, the fatty acid precipitates as nanoparticles owing to proton exchange between the acid solution and the sodium salt.

SLN were prepared using two different positive-charged substances: ST or GCS. ST possess a hydrocarbonic chain that can probably be incorporated within the lipid matrix, while its positive charge is exposed to the external surface. GCS, a chitosan derivative conjugated with ethylene glycol branches, is a water soluble at a neutral/acidic pH values polymer whose pendant glycol branches increase both the aqueous solubility of the native chitosan (CS) and provide steric

7

166   stabilization [36]. Mao et al [37] have established that CS is capable of opening the tight junctions

167   of epithelial cells and it can improve the uptake of hydrophilic drugs including peptides.

168   For the above mentioned purpose, PTX loaded cationic SLN were prepared and extensively

169   characterized *in vitro* with regard to their physicochemical properties, their capacity to load and

170   release PTX, their cytotoxicity and their permeability across hCMEC/D3 cell lines taken as an *in*

171   *vitro* model of BBB.

2. Experimental

2.1 Chemicals

Sodium Behenate (Na-BA) was purchased from Nu-Chek Prep, Inc. (Elysian, U.S.A.), Tween®80, sodium dodecyl sulfate, Triton X-100 and cholesterol from Fluka (Buchs, Switzerland), paclitaxel (PTX) from Indena (Milan, Italy), citric acid from A.C.E.F. (Fiorenzuola d'Arda, Italy), 80% hydrolyzed PVA 9000–10000 Mw (PVA 9000), Pluronic F68, stearylamine (ST), glycol chitosan (GCS), coumarin 6 (Cou-6), triethanolamine phosphate, trehalose, penicilin-streptomycin, hydrocortisone, ascorbic acid, Hepes and b-FGF from Sigma (Dorset, UK), hydrochloric acid, sodium hydroxide and sodium phosphate monobasic from Merck (Darmstadt, Germany), Cremophor® EL from BASF (Ludwigshafen am Rhein, Germany), EBM-2 basal medium from Lonza, (Basel, Switzerland), fetal bovine serum Gold from PAA The Cell Culture Company (Pasching, Austria), rat collagen-I from Trevigen (Gaithersburg, Maryland, USA), chemically defined lipid concentrate from Invitrogen Life technologies (Carlsbad, California, USA), methanol and ethanol from Carlo Erba (Val De Reuil, France). Deionized water was obtained by a MilliQ system (Millipore, Bedford, MO).

2.2 hCMEC/D3 cells

hCMEC/D3 cells, a primary human brain microvascular endothelial cell line that retains the property of BBB *in vitro*, were cultured as reported [38]. Briefly, cells were maintained in Petri dishes coated with 150 µg/ml rat collagen-I and cultured in EBM-2 basal medium supplemented with 5% v/v fetal bovine serum Gold, 1% v/v penicilin-streptomycin, 1.4 µM hydrocortisone, 5 µg/ml ascorbic acid, 10 mM Hepes, 1% v/v Chemically Defined Lipid Concentrate, 1 ng/ml b-FGF. In all the experiments cells were used between passages 29 and 34. For the permeability assays, cells were seeded at 50,000/cm² and grown for 7 days up to confluence in Petri dishes and Transwell devices (0.4 µm diameter pores-size, Corning Life Sciences, Chorges, France), with 1.5

197   ml/cm^2 and 3 ml/cm^2 of the culture medium described above in the Transwell insert and in the

198   lower chamber, respectively.

199   Before each experiment we measured the transendothelial electrochemical resistance (TEER) and

200   the permeability coefficient of dextran-FITC, [^{14}C]-sucrose and [^{14}C]-inulin, taken as parameters

201   of paracellular transport across hCMEC/D3 monolayer, as described in [39]. TEER value was

202   between 30 and 40 Ω x cm^2, dextran-FITC permeability coefficient was 0.015 ± 0.003 x 10^{-3}

203   cm/min, [^{14}C]-sucrose permeability coefficient was 1.19 ± 0.21 x 10^{-3} cm/min, [^{14}C]-inulin

204   permeability coefficient was 0.56 ± 0.09 x 10^{-3} cm/min. These values suggested the functional

205   integrity of BBB monolayer [38].

206

207   *2.3 GBM cell lines and culture conditions*

208 Primary human GBM cell lines NO3 and CV17 were obtained from primary human GBMs

209 surgically resected at the Department of Neuroscience, Neurosurgical Unit, University of Turin,

210 Italy. The histological diagnosis was performed according to World Health Organization (WHO)

211 guidelines. The study was in compliance with the local institutional review board and Committee on

212 Human Research and with the ethical human-subject standards of the World Medical Association

213 Declaration of Helsinki Research. Written informed consent was obtained from all patients.

214 010627 GBM cell line was a kind gift of Dr. Galli R, DIBIT San Raffaele, Milan, Italy). For

215 cytotoxicity studies in co-culture models U87-MG cells (ATCC, Rockville, MD) were also used.

216 By neurosphere assay, from a resected tumor tissue we obtained neurosphere (NS) or adherent cell

217 (AC) or both cell types [40]. NS lines were cultured on Dulbecco's modified Eagle's medium

218 (DMEM)/F-12 supplemented with 20 ng/ml epidermal growth factor (EGF) and 10 ng/ml basic

219 fibroblast growth factor (bFGF); AC lines were grown on DMEM supplemented with 10% fetal

220 bovine serum (FBS) for AC. Both cultures were maintained at 37°C and at 5% O_2/CO_2 in a

221 humidified multigas Sanyo MCO-18M incubator (Sanyo Scientific, Bensenville, IL).

222   All cell cultures were periodically checked for *Mycoplasma* contamination (e-Myco[TM]

223   Mycoplasma PCR Detection kit, iNtRON Biotechnology, Korea).

224

225   *2.4 PTX-loaded SLN preparation*

226   Different SLN formulations were prepared (Table 1); non-charged SLN were prepared as reference

227   to evaluate the positive-charge influence.

228   Non-charged SLN**:** SLN were prepared by the coacervation method [35]. Briefly, appropriate

229   amounts of Na-BA and PVA 9000 were dispersed in 5 ml deionized water and the mixture was then

230   heated under 5 min-stirring (300 rpm) just above the Krafft point of Na-BA (75 °C) to obtain a clear

231   solution (micellar solution). A selected acidifying solution (100 µl 1M NaH_2PO_4 + 160 µl 1M HCl)

232   was then added drop-wise until pH 4.0 was reached. The obtained BA SLN suspension was then

233   cooled in a water bath under 10 min-stirring at 300 rpm until 15 °C temperature was reached. SLN

234   suspension was then again heated under stirring (300 rpm) just above the melting point of BA (80

235   °C). Different amounts of 30 mg/ml ethanol PTX solution, heated at the same temperature of SLN

236   suspension, were added to the warm mixture and then the sample was again cooled in a water bath

237   under stirring at 300 rpm until 15 °C was reached.

238   Charged SLN**:** SLN were prepared as described for non-charged SLN, introducing the positive-

239   charged agent as follows:

240   -   ST-SLN**:** a fixed amount of 30 mg/ml 2-propanol ST solution (Table 1) was added to the warm

241   aqueous Na-BA solution just above the Krafft point of Na-BA.

242   -   GCS-SLN**:** an appropriate amount of GCS (Table 1) was added at the beginning of the

243   preparation before obtaining the micellar solution.

244   All SLN formulations were also prepared in the presence of cholesterol (CHOL-SLN): 100 or 150

245   µl of 5 mg/ml ethanol CHOL solution were added to the micellar solution immediately before the

246   addition of the acidifying solution.

247 All SLN formulations were also prepared without drug (unloaded SLN) adding the same amount of

248 ethanol instead PTX-ethanolic solution.

249 Fluorescent SLN to be employed in *in vitro* experiments were prepared using Cou-6 as fluorescent

250 lipophilic model drug (Cou-6-CHOL-SLN). 5 ml SLN were prepared in aseptic conditions (under

251 laminar flow airfilter starting from materials sterilized with UV or in autoclave) adding 100 µl

252 2mg/ml Cou-6 ethanol solution after SLN fusion. The samples were then cooled in a water bath

253 under stirring at 300 rpm until 15°C temperature was reached.SLN were lyophilized using a

254 programmable freeze-dryer (Shin PVTFD10R, Shinil Lab, Korea) without cryoprotectant addition.

255 Slow freezing was carried out on the shelves in the freeze dryer (shelf temperature −40 °C).

256 Samples were lyophilized for 24 h from −40 °C to 25 °C at a 5 °C/h. increasing rate. Lyophilized

257 products were reconstituted by magnetic stirring adding the same water amount.

258

259 *2.5 SLN characterization*

260 SLN shape and mean sizes were characterized by Transmission electron microscope (TEM, CM 10

261 Philips, The Netherlands) spraying the SLN suspension on the microscope grid by means of an

262 aerosol-sampling device.

263 Cou-6 localization into SLN dispersion was determined using optical microscopy equipped with a

264 fluorescent lamp (Leica DM 2500, Solms, Germany) at 1000x magnification.

265 SLN particle sizes, polydispersity indexes (PDI) and Zeta potential were determined one hour after

266 preparation using laser light scattering technique-LLS (Brookhaven, New York, USA). Size

267 measurements were obtained at an angle of 90° at 25 °C using the number method. The dispersions

268 were diluted with water for size determination or with 0.01 M KCl for Zeta-potential determination,

269 in order to achieve the prescribed conductibility. Size measurements were also recorded diluting

270 samples with grown medium used to culture hCMEC/D3 cells to mime the conditions under which

271 SLN undergo in vitro experiments. For stability studies, the samples were stored at 4°C. All data

272 were determined in triplicate.

PTX entrapment efficiency (EE%) was calculated as the ratio between PTX amount in SLN and that in the starting micellar solution $\times$ 100. PTX EE% determination was performed as follows: 1 ml SLN suspension was centrifuged for 15 min at 62,084 g, the precipitate was washed twice with 1 ml ethanol:water 30:70 to eliminate adsorbed PTX. The solid residue was dissolved in 1 ml ethanol, 0.5 ml water were then added to precipitate the lipid matrix and the supernatant obtained was injected in HPLC for PTX quantification.

EE% was also determined after 1:100 dilution in different media to mime the dilution that SLN can undergo after administration. Briefly, 500 µl SLN were introduced in a 50 ml flask and 49.5 ml water or 0.1 M phosphate buffer pH 7.4 or 0.1 M citric acid buffer pH 5.5 were added. The suspension was stirred for 2 hours. 8 ml suspension were centrifuged for 15 min at 62,084 g and then treated as previously described.

2.6 HPLC analysis

HPLC analysis was performed using a LC9 pump (Shimadzu, Tokyo, Japan) with a Chromosystem™ ODS 2.5 µ 125×4.6mm column and a C-R5A integrator (Shimadzu, Tokyo, Japan); mobile phase: $CH_3CN:H_2O$ 60:40 (flow rate 1ml min^{-1}); detector: UV λ=227 nm (Shimadzu, Tokyo, Japan). Retention time was 2.6 min.

The limit of quantification, defined as the lowest PTX concentration in the curve that can be measured routinely with acceptable precision and accuracy, was 0.013 µmol/ml; the limit of determination, defined as the lowest detection limit, was 0.005 µmol/ml (signal to noise>2.0).

2.7 SLN and PTX stability

SLN sizes and PTX EE% of samples stored at 4 °C were monitored for 90 days to study SLN physical stability and PTX chemical stability. Mean sizes were determined by LLS and PTX EE% over time was obtained as described by HPLC.

298 The same SLN suspensions were freeze-dried without adding any cryoprotectant (FD-SLN) using a

299 Modulyo Freeze Dryer (Edwards Alto Vuoto, Italy). The resulting samples, rehydrated with the

300 same water amount, were also characterized by size, Zeta potential and EE% determination.

301

302 *2.8 PTX in vitro release*

303 *In vitro* release of PTX was determined using the non-equilibrium dialysis method [41]. A

304 multicompartmental rotating cell system consisting of donor and receptor compartments of equal

305 volume (1.5 ml) separated by a dialysis membrane (cut-off 12,000 Da) was used. Receiving

306 medium was 0.1 M phosphate buffer (pH 7.4) containing 0.1% v/v Tween®80. Solution of PTX in

307 receiving medium and SLN suspensions were used as donor formulations. At fixed times, the

308 receptor solution was tipped out and used for HPLC analysis and the cell was refilled with fresh

309 receiving medium. Drug concentration was determined by HPLC. The results were evaluated as

310 PTX apparent permeability constant (Kd_{app} [cm h^{-1}]) calculated from the slope of the straight line

311 obtained by plotting the amount of PTX diffused from the donor formulation versus time, assuming

312 pseudo zero-order kinetics.

313

314 *2.9 Permeability of SLN through hCMEC/D3 cell monolayer*

315 hCMEC/D3 cells, seeded as reported above in Transwell devices, were incubated at day 7 with

316 SLN 2, SLN 9, SLN 15 loaded with Cou-6, for 0.5, 3 and 24 h in the Transwell

317 insert. The amount of SLN added was 100 µl diluted with 900 µl of medium. This dilution of

318 SLN was the highest concentration devoid of cytotoxic effects on hCMEC/D3 cells, as previously

319 reported [42]. In parallel, a set of Transwell inserts were incubated with Cou-6 aqueous suspension

320 obtained with PVA 9000 as suspending agent, containing the same concentration of Cou-6

321 present in SLN. At the end of the incubation time, the medium in lower chamber was collected,

322 diluted 1: 20 into ethanol, sonicated with 10 bursts of 1 s to disrupt SLN, and centrifuged at 62,084

323 g for 5 min, to pellet debris. The dilution of the medium was necessary to obtain a fluorescence

14

324   falling in the detection range of the LS-5 spectrofluorimeter (PerkinElmer, Waltham, MA), used to

325   measure the fluorescence of Cou-6.

326   Excitation and emission wavelengths were 485 ± 20 nm and 528 ± 20 nm, respectively. The

327   fluorescence of Cou-6 at t_0 in the upper chamber, was considered 100%. The fluorescence of Cou-6

328   measured in the medium collected from the lower chamber was expressed as percentage of

329   fluorescence in the upper chamber at t_0. The fluorescence of the medium without Cou-6 was

330   considered as blank and was subtracted from the fluorescence of all the other experimental

331   conditions.

332   To measure the amount of Cou-6 adsorbed on the Transwell membrane, Cou-6, either free or loaded

333   in SLN, was added in empty Transwells in the same experimental conditions of the Transwells

334   containing hCMEC/D3 cells, then the medium from the insert and the lower chamber was removed;

335   the Transwell membrane was washed with PBS and 0.5 ml ethanol was added to solubilize the

336   Cou-6 adsorbed on the membrane. The solution was collected and its fluorescence was read as

337   reported above. The fluorescence was always less than 4% of the fluorescence measured in the

338   lower chamber medium in all the experimental conditions, suggesting that such very low absorption

339   of Cou-6 on the Transwell insert did not influence the results of the permeability assays.

340   The level of significance was determined by a Student's *t* test. Statistical significance was defined

341   as $p < 0.001$.

342

343   *2.10 In vitro cytotoxicity assay*

344   For cytotoxicity studies, NO3 cells (both NS and AC) and CV17 NS were used at various passage

345   numbers between 20 and 30, whereas 010627 cells (both NS and AC) were used at passage

346   numbers between 160 and 180.

347   Free PTX (Sigma Aldrich Co., St. Louis, MO, USA) was dissolved in 100% DMSO for stock

348   solutions and dilutions for cell treatments were made extemporaneously in culture medium, so that

349   the final concentration of DMSO never exceeded 0.3% (v/v).

Cell lines were treated for 72 h with increasing doses (20, 100, 500, 1400 nM) of free PTX.

After exposure the cytotoxic effect of free Paclitaxel (PTX) and PTX-loaded SLN against tumor cells was evaluated assessing the number of viable cells by the Trypan blue dye exclusion test, using a TC20 automated cell counter (Bio-Rad, Berkeley, CA, USA). As for AC, results were confirmed by the 3-(4,5-dimethylthiazol-2-yl)-2,5-diphenyl-tetrazolium bromide (MTT) assay (Roche, Diagnostic Corporation Indianapolis, IN, USA) [43].

For Trypan blue assay, cells were plated at a density of 200×10^3 cells in 5 ml medium in a 25 cm^2 flask and treated with PTX (free in solution or encapsulated in SLN2, SLN9 or SLN15) at 37°C in 5% O_2/CO_2 for different times (24 and 72 h). Stock solutions were diluted extemporaneously in fresh medium at the desired concentration and administered to cells.

Cytotoxicity was expressed as number of surviving cells as percentage of control (untreated cells). For MTT assay, cells were seeded in 96-well plates (1 x 10^4 cells/well in 100 µl medium) and treated with the different concentrations and times above indicated of the drug (free or encapsulated) at 37 °C in 5% O_2/CO_2. The medium with the SLN was replaced with fresh medium and 10 µl of MTT solution (5mg/ml) were added to each well and incubated for 4 h at 37 °C. The extent of cell viability is indicated by mithocondrial conversion of yellow MTT, a tetrazole, to purple formazan by the living cells. Formazan crystals were solubilized overnight in 10% sodium dodecyl sulfate (SDS), 0.01 M HCl and optical density was measured at 570 nm (test wavelength) and 660 nm (reference wavelength) using a microplate spectrophotometer (Synergy HT, BioTek Instruments Inc., Winooski, VT, USA). Cell viability was expressed as a percentage of the absorbance measured in the treated cells compared to the control (untreated cells). All experiments were performed in quadruplicate.

The concentration of free PTX which caused a 50% cell growth inhibition (IC_{50}) compared with untreated controls, was calculated by non-linear regression for each cell line.

To investigate the cytotoxic effect of PTX incorporated in SLN, a drug concentration of 100 nM was chosen for the following *in vitro* experiments.

376 Cell viability was also measured after treatment with unloaded SLN (SLN2, SLN9 and SLN15) at

377 the highest SLN concentration used for the study, *i.e.* 0.1% w/v.

378 The level of significance was determined by a two-tailed Student's *t* test. Statistical significance

379 was defined as $p < 0.05$ or $p < 0.01$.

380

381 *2.11 DNA damage/repair study by Immunofluorescence (IF)*

382 The occurrence of a DNA damage after SLN treatment was investigated through the analysis by IF

383 of γ-H2AX histone, that localizes at sites of DNA fragmentation as subnuclear foci.

384 The cell response to DNA insults was studied monitoring the activation of p-ATM, p-Chk2 and p-

385 53BP1. HR or NHEJ repair system activities were analyzed through RAD51 or Ku70/Ku80 and

386 DNA-PKcs proteins respectively. After 72 h treatment with unloaded SLN (SLN9) or with 100 nM

387 PTX-loaded SLN9, cells were fixed for 20 minutes with 4% paraformaldehyde at room

388 temperature, rinsed three times with PBS, blocked/permeabilized with PBS containing 2% of the

389 appropriate serum and 0.1% Triton X-100 for 30 minutes and stained with the following primary

390 antibodies: mouse anti-γ-H2AX (Ser139), mouse anti-p-ATM (Ser1981) (both from Millipore),

391 rabbit anti-p-Chk2 (Thr68) (Cell Signaling Technology), rabbit anti-p-53BP1 (Ser25) (Bethyl

392 Laboratories), mouse anti-RAD51, mouse anti-DNA-PKcs and mouse anti-Ku70/Ku80 (all from

393 NeoMarkers). Negative controls were obtained by omitting the primary antibody. Alexa Fluor®

394 488-AffiniPure goat anti-rabbit IgG and Alexa Fuor® 594-AffiniPure rabbit anti-mouse IgG

395 (Jackson ImmunoResearch Laboratories, Inc., West Grove, PA, USA) were used as secondary

396 antibodies. Cell nuclei were counterstained with 4',6-diamidino-2-phenylindole (DAPI) and

397 observations were made under a Zeiss Axioskop fluorescence microscope (Karl Zeiss, Oberkochen,

398 Germany) equipped with an AxioCam5MR5c and coupled to an Imaging system (AxioVision

399 Release 4.5; Karl Zeiss).

400

401 *2.12 Specimen preparation for transmission electron microscopy (TEM)*

17

Analysis by TEM was employed in order to get information on the possible ultrastructural modifications of cells treated with empty and PTX-loaded SLN. NO3 NS and AC lines were used for the investigation.

For transmission electron microscopy, untreated cells, cells treated with unloaded SLN15 and cells treated with 100 nM PTX-loaded SLN15 for 24 h were collected, pelleted by centrifugation and then fixed with 2.5% glutaraldehyde prepared in 0.1 M phosphate buffer at 4 °C. Samples were post-fixed with 1% osmium tetroxide for 2 h, dehydrated in a graded acetone series and embedded in the Epon 812 epoxy resin. Ultrathin sections were prepared using an ultracut microtome (Reichert-Jung, Germany), collected on copper grids, stained with both lead citrate and uranyl acetate, and then observed with a Philips CM-12 transmission electron microscope.

2.13 Glioblastoma cell cytotoxicity in co-culture models

In co-culture experiments, 500,000 glioblastoma cells (i.e. the U87-MG cell line and the primary human glioblastoma cells CV17 and 01010627) were added in the lower chamber of Transwells 4 days after seeding hCMEC/D3 cells in the upper chamber of Transwells. After 3 days of co-culture the medium of the upper chamber was replaced with fresh medium, with or without free PTX or PTX-loaded SLN (SLN 2) at different concentration (20, 50, 100, 200, 500 nM) for 24 h, as detailed under results.

To measure the viability of glioblastoma cells co-cultured with hCMEC/D3 cells, extracellular medium of glioblastoma cells was collected and centrifuged at 12,000 g for 15 min to pellet cellular debris, whereas cells were washed with fresh medium, detached with trypsin/EDTA (0.05/0.02% v/v), re-suspended in 0.2 ml of 82.3 mmol/l triethanolamine phosphate-HCl (pH 7.6) and sonicated on ice with two 10 s bursts (Labsonic sonicator, 100 W). LDH activity was measured in the extracellular medium and in the cell lysate: 50 μl of supernatant from extracellular medium or 5 μl of cell lysate were incubated at 37 °C with 5 mmol/l NADH. The reaction was started by adding 20 mmol/l pyruvic acid and was followed for 6 min, measuring absorbance at 340 nm with Packard

428   EL340 microplate reader (Bio-Tek Instruments, Winooski, VT). The reaction kinetics was linear

429   throughout the time of measurement. Both intracellular and extracellular enzyme activity was

430   expressed in μmol NADH oxidized/min/dish, then extracellular LDH activity was calculated as

431   percentage of the total LDH activity in the dish.

432   The level of significance was determined by a Student's *t* test. Statistical significance was defined

433   as $p < 0.05$, $p < 0.02$, $p < 0.01$, $p < 0.005$ or $p < 0.001$.

3. Results and discussion

As described in the introduction chapter, BBB is a physical barrier characterized by tight intracellular junctions and by the absence of fenestrations that limit permeability for therapeutic molecules with no exception for molecules in the glioblastoma treatment. The use of drug-loaded nanoparticles could be a winning strategy if an active targeting and a suitable drug concentration to the brain could be obtained, provided small-sized hydrophilic vehicles are achieved to prevent rapid degradation by reticuloendothelial system and carriers with proper superficial characteristics are coupled.

Moving from this background, SLN were prepared using the coacervation method which uses hydrophilic polymeric as stabilizers able to confer hydrophilic surface to SLN. Further to a cytotoxicity study against hCMEC/D3 cells relating to different fatty acids [40], BA was chosen as lipid matrix. In order to take advantages of possible interaction between BBB negative charges and surface positive-charged SLN, two positive charged molecules currently used in literature were introduced in the SLN preparation: ST [44] and GCS [36]. As antineoplastic model drug PTX was chosen, a lipophilic molecule suitable to be entrapped in SLN matrix.

Preliminary formulation studies (data not reported) demonstrated the need to modify the preparation procedure to obtain higher drug EE% by introducing PTX after SLN melting instead of adding it to the micellar solution; probably the high PTX lipophilicity does not allow its distribution within micelles, while promoting its solubilization in the molten lipid.

3.1 SLN characterization

In Table 1 compositions of PTX-loaded SLN are reported. SLN composition was the result of a preliminary screening carried out in a previous work [45].

In Table 1 ST-SLN and GCS-SLN compositions are also reported. Different formulations were obtained varying the amount of PVA 9000, ST, GCS or PTX in order to obtain the most suitable PTX vehicle as concerns Zeta potential, mean sizes, EE%, over time stability. In order to improve

SLN stability, CHOL was also added. As reported in literature [46] high CHOL/lipid ratio matrix reduced mean diameters of SLN prepared from emulsion. This led to a rigid surfactant layer with decrement in van der Waals attraction and promotion of net repulsion forces between oil droplets; therefore, agglomeration and coalescence of small oil droplets were reduced. In addition, the interaction between CHOL and surface active agent might increase the surface curvature of oil droplets consequently leading to small size of SLN after cooling down. A similar behavior can be hypothesized also in SLN obtained by coacervation. In the present experimental conditions, CHOL probably might interact with Na-BA at the interface of micelles.

In Table 1 SLN, ST-SLN and GCS-SLN mean diameter and Zeta potential are reported. Most SLN tested had sizes below 600 nm. In the neutral SLN series (SLN 0-3), increasing the amount of PTX no changes in particles dimension were noted; different behavior was noted in the case of charged SLN. In the ST-SLN series (SLN 4-10) an increase in diameter sizes can be noted when ST or PTX amounts were increased or when CHOL was introduced in the formulation. Nevertheless the presence of CHOL was essential to SLN stability: in the absence of CHOL, ST-SLN and GCS-SLN showed a sudden increase in mean size immediately after preparation. Instead, in the GCS-SLN (SLN 11-17) series a slightly decrease in SLN size was obtained increasing the GCS amount and a more marked increase was noted when a great amount of stabilizer (PVA) was used. Also in this case the presence of CHOL was necessary to formulations stability; the addition of this component led to a decrease in mean diameter and the smallest SLN were obtained using 50 mg (1% w/w) PVA (SLN 17).

The dissimilar influence of ST and GCS on ST-SLN and GCS-SLN sizes might be due to different positioning of both charged molecules: probably, lipophilic ST chain was incorporated in the lipid matrix while GCS was mainly adsorbed to the external surface of nanoparticles.

Size measurements were employed also diluting the samples with growth medium used in the in vitro experiments in order to verify SLN sizes when they are tested in vitro. The growth medium does not seem to influence SLN dimensions: all SLN have maintained their size (data not reported).

21

In Figures 1a and 1b TEM PTX-SLN2 images at different magnifications were reported. The SLN have spherical shape and sizes between 300 and 500 nm. The drug introduction does not seem to affect shape and size (data not reported). Similar characteristics were obtained also with SLN9 and SLN15.

The observation of Cou-6-SLN nanosuspensions under optical microscope confirmed both the spherical shape and the dimensional range of the particles. The use of fluorescent light allowed to locate Cou-6 in SLN nanosuspensions: homogeneous dispersions of fluorescent nanoparticles were observed with all formulations (data not shown).

In Table 1 also Zeta potential values are reported. All GC or ST-containing formulations showed positive charge with values in the 7.6 - 23.8 mV range. ST-SLN presented Zeta potential ranging from 7 to 15 mV (depending on ST amount used); these values are smaller than those of GCS-SLN and those of SLN containing the same ST percentages but prepared with methods other than coacervation [41]; probably PVA 9000 used as stabilizer locates itself externally thus partially screening the ST positive charge.

In GCS-SLN series, Zeta potential values confirmed the external positioning of the polymer: probably positively-charged GCS interacted with carboxylate groups on SLN surface, conferring them a positive charge. The values were influenced by GCS amount: by increasing the polymer an increase of Zeta potential from 16.9 mV to 23.8 mV was noted; the presence of CHOL and the PTX amount variation did not seem to influence this parameter.

In Table 2 the amount of PTX in SLN is expressed as EE% and as loading (mg PTX/mg BA). Almost all tested SLN showed a good PTX loading capacity; in particular, in neutral SLN series (SLN 0-3) PTX EE% did not significantly vary increasing the drug amount, while drug loading was increased over twice folds. In the ST-SLN series (SLN 4-10), PTX EE% was significantly influenced by several factors. Increasing ST amounts determined a reduction of PTX EE% (SLN 5) which was partially counteracted by the presence of CHOL (SLN 6) probably as a consequence of a

22

511   hardened structure of SLN surface. Also PVA amount seemed to be relevant in influencing PTX

512   EE%, as higher PVA concentrations determined a reduction in PTX EE%.

513   In GCS-SLN series (SLN 11-17), EE% and PTX loading ranged from 24% to 83% and from 1.4 to

514   5.0 mg/mg BA respectively. Also in this series PTX EE% was strongly influenced by PVA 9000

515   amount: when the highest stabilizer amount was used (SLN 14), a dramatic decrease in drug EE%

516   up to 24% can be noted; probably PVA 9000 formed micelles in aqueous phase able to solubilize

517   PTX. CHOL introduction enhanced PTX EE% from 52% to 75% particularly in SLN prepared with

518   50 mg PVA 9000. On the contrary, GCS amount variations did not seem to affect drug EE%.

519   To mime SLN behavior after administration when they are diluted in physiological fluids, drug

520   EE% was determined also after 1:100 dilutions. When water was used as dilution medium, EE%

521   remained almost unvaried in all ST-SLN (±1%), except in SLN 15 in which a 10% decrease was

522   registered. Probably, in GCS-SLN, PTX is partially trapped in GCS chains located on SLN surface

523   and therefore it might be released upon high dilutions. To evaluate the influence of different

524   dilution media, SLN 9, which were chosen as those having the best properties for our experimental

525   purposes, were diluted also by pH 7.4 PBS and pH 5.5 citric buffer. No significant variation was

526   noted upon dilution by pH 7.4 PBS (±1%), while a certain PTX amount was released when 0.1

527   citric pH 5.5 buffer was used, that mimed the lysosomial environment: the EE% decreased from

528   92% to 77% and this could be due to a PTX slow release.

529

530   *3.2 SLN and PTX stability*

531   The studies were carried out only on SLN giving the best results concerning sizes and EE%. The

532   chosen formulations were analyzed to verify their stability overtime. The results are reported in

533   Table 3. SLN 9 showed a great increase in mean diameter (up to 1500 nm) after 30 days, while only

534   a slight decrease occurred in EE%. The poor dimensional stability of SLN 9 could be due to their

535   low Zeta potential (about 9 mV) which is probably not sufficient to prevent SLN aggregation. On

536   the other hand, GCS-SLN (SLN 15, 16, 17) showed a higher dimensional stability although a

gradual increase in mean diameter and a gradual decrease in Zeta potential were registered due

probably to a slow solubilization of the external GCS coating in the aqueous phase.

To overcome the poor stability of SLN suspension and to find an optimal storage method, they were

submitted to freeze drying. In Table 4 SLN sizes after freeze-drying were reported. The freeze-

drying process was carried out without adding any cryoprotectant; in fact in a previous work [45]

PVA 9000 was found to be able to protect SLN during freeze-drying as well as 2% threalose.

The characterization of resulting SLN suspensions showed a mean diameter increase of all SLN

analyzed probably due to a partial SLN aggregation. This increase was about 300 nm in SLN with

ST while only a slight variation was registered in SLN with GCS; probably also GCS, positioning

externally, could behave as cryoprotectant preventing nanoparticles aggregation. The smallest

increase (about 40 nm) was noted when higher amounts of stabilizer were used. EE% was kept

constant in almost all preparations; an increase in EE% (from 75% up to 89%) was registered in

SLN 17 that presented a higher amount of free PTX: probably during freeze-drying a part of free

PTX was internalized or absorbed onto nanoparticles.

3.3 Determination of PTX release

In Figure 2 PTX release plots from SLN using the dialysis method were reported. In this experiment

drug diffusion through the dialysis membrane was influenced by drug release rate from SLN. As it

can be seen, PTX was released very slowly from SLN: less than 1% PTX was released from SLN

formulations in 12 hours while, at the same time, about 40% PTX diffused from PTX solution. This

slow release could confirm PTX incorporation into SLN. From the $K_{d\ app}$ data it could be seen as

PTX release from GCS-SLN was still slower than from ST-GCS; these results could be the

confirmation that GCS formed an external coating that further limited drug release.

3.4 Permeability of SLN across BBB

As shown in Figure 3, the permeability of free Cou-6 across the hCMEC/D3 monolayer remained very low at all the time points considered; the permeability of Cou-6-loaded SLN was similar to that of free Cou-6 after 0,5 h, but became significantly higher after 3 h and 24 h. Apparently there were no differences in the permeability of uncharged SLN (SLN 2) versus positively charged SLN (SLN 9 and SLN 15), although SLN 9 resulted the best permeable formulation after 24 h.

3.5 In vitro cytotoxicity studies

To assess the sensitivity of the five malignant glioma cell lines to PTX, we treated previously the cells with Cremophor® EL:ethanol 50:50 drug solution (free PTX) at concentrations ranging from 20 nM to 1.4 µM for 72 h.

After different exposure times both MTT and trypan blue assays were performed. PTX was able to block *in vitro* cellular proliferation in a dose-dependent manner; it inhibited clonogenic growth of NS (Figure 4a–4d) and hindered adhesion process in AC (Figure 4e–4i).

The growth inhibitory effect was more evident on AC than on NS.

The IC_{50} values of free PTX at 72 h for the three NS cell lines studied were < 20 nM; for the two AC lines were < 15 nM (Figure 5). Consequently, drug concentration of 100 nM was employed for the following experiments with PTX incorporated in SLN. At this dosage, a statistically significant decrease of cell viability was caused by PTX compared with untreated cells, both as free drug and as SLN-carried, and this effect increased prolonging drug exposure time from 24 to 72 h. It was observed that also PTX encapsulated in SLN caused inhibition of sphere formation in the NS cultures (Figure 4e) and interfered with cell adhesion in AC cultures (Figure 4l).

Graphs in Figure 7 show cell viability of NO3 line after the treatments: as regards NS, the viable cell number decreased to 60-70% after 24 h treatment with the different PTX-SLN (Figure 6a) and to 30-40% after 72 h treatment (Figure 6b). At 24 h free PTX and all PTX-SLN gave a cytotoxicity statistically different from control, while only SLN 2 produced an increase in cytotoxicity

significantly different from that of empty SLN 2. Prolonging the incubation time, also SLN 9 were

significantly different from the corresponding empty SLN.

The reduction of viability of AC was about 10-15% higher than the one of NS (Figure 7). An

analogous behavior of PTX-SLN 2 and PTX-SLN 9 was noted already after 24 h incubation, while

after 72 h all SLN under study produced a cytotoxicities significantly different from those produced

by the corresponding empty SLN. The cytotoxicity of PTX incorporated in SLN appeared similar

or even slightly higher in comparison with the one of free drug solution. In particular, SLN2 seemed

to enhance growth inhibitory activity of PTX on NS lines, while SLN 9 did it on AC lines.

The results slightly varied in the other cell lines (data not shown), but the cytotoxic activity of PTX-

loaded SLN remained always equal or greater compared with free drug. SLN 2 and SLN 9 appeared

as the most effective carrier formulations.

Control experiments demonstrated that the exposure of the cells with the unloaded SLN at the

highest SLN concentration used for the study determined a mild reduction of cell viability too,

mostly on AC. Unloaded SLN 2 formulation displayed the smallest cytotoxic effect, while unloaded

SLN15 had a more accentuated action on cell proliferation.

Treatment with PTX vehicle (50:50 v/v mixture of Cremophor® EL and ethanol) at the same

concentrations used for drug solutions showed a slight cytotoxicity too (data not reported).

Our results suggest that, first of all, incorporation of PTX in SLN did not alter its cytotoxic

capability and that these carriers, thanks to a good cell membrane permeation, are able to efficiently

transport the drug inside the cells. Encapsulation into SLN appeared even to enhance the growth

inhibitory effect of PTX on GBM cell lines.

In conclusion, loading of PTX in SLN seems to sensitize cells and to decrease their resistance to the

drug.

3.6 Study of PTX-SLN cytotoxic effect by TEM

26

The observation by TEM enabled to evaluate the ultrastructural alterations of cells after exposure to SLN. The analysis revealed that the administration of unloaded SLN 15 didn't cause modifications to the cell morphology both in NS and in AC. Cells treated with empty SLN maintained unchanged nucleus, ergastoplasma, Golgi apparatus and mithocondria (Figure 8a).

On the contrary, 24 h exposure to SLN loaded with 100 nM PTX induced severe alterations of the cellular morphology that included cytoplasmic accumulation of vacuoles, loss of mitochondrial ridges and finally mithocondrial lysis (Figure 8b-8f). The vacuoles became gradually larger and confluent and in some cases they blended and formed autophagolysosomes surrounded by a membrane. Cytoplasmic rarefaction, glycogen accumulation and destruction of all organelles suggested a typical regressive apoptotic pattern. Only in some areas there was evidence of SLN residues. These results indicate an evident cell damage caused by the PTX vehicled in the SLN.

3.7 DNA damage and repair response induced by PTX-SLN treatment

In response to DNA damage caused by genotoxic agents, the eukaryotic cell activates a complex checkpoint/repair pathway in order to repair the lesion before replication. The signalling involves the recruitment of the sensor protein kinase ataxia telangiectasia mutated (ATM), that initiates a transduction cascade phosphorylating downstream effectors, including H2AX histone, 53 binding protein 1 (53BP1) and the checkpoint kinases 1 and 2 (Chk1 and Chk2). When checkpoints are activated, the cell cycle is halted to allow DNA repair. If the damage is too severe, repair fails and the cell enters into apoptosis [47]. Two are the major pathways used by mammalian cells to repair double strand break damage: the homologous recombination (HR), which takes place during the S and G2 phases and is driven mainly by RAD51 protein, and the non-homologous end joining (NHEJ), which occurs during G0 and G1 phases. The key NHEJ effector is DNA-dependent protein kinase (DNA-PK), which consists of a regulatory subunit (Ku70/Ku80 heterodimer) and a catalytic subunit (DNA-PKcs) [48]. In glioma cells, increased DNA damage response and repair ability contribute to determine the radio- and chemoresistant phenotype of these cells [49].

After glioma cell treatment for 72 h with relatively high concentration (100 nM) of free PTX we observed a moderate activation of checkpoint and repair proteins. A mild expression of all markers, was found both in NS and in AC (data not shown), indicating that this drug is able to induce genotoxic lesions.

Even after NO3 cell line treatment with PTX carried by SLN, we found the presence of γ-H2AX positive-nuclei and a moderate expression of all sensors and effectors of checkpoint/repair pathway, both in NS (Figure 9a-9g) and in AC (Figure 9l-9q), demonstrating that the encapsulated drug maintains the ability to induce a DNA strand break damage in the glioma cell lines. As already observed for the free drug, mostly on AC lines, several cells treated with PTX-SLN appeared blocked in metaphase (Figure 9i) and presenting a strong expression of the checkpoint/repair proteins (p-ATM, p-Chk2, p-53BP1, γ-H2AX, DNA-PKcs). It seemed from these findings that cells try to repair the genotoxic lesions mainly through the NHEJ system. Untreated cells were negative for all markers (inserts in Figure 9a and 9i are examples for p-ATM expression).

After exposure of cells to unloaded SLN for 72 h we did not observe positivity of any checkpoint/repair protein (panels h and r of Figure 9 are examples for p-ATM expression).

3.8 Effective cytotoxicity of paclitaxel-loaded SLN against glioblastoma cells in co-culture models.

The cytotoxicity of PTX-loaded SLN on glioblastoma cells was finally compared with that of free PTX in co-culture models of hCMEC/D3 cells and glioblastoma cells. As shown in Figures 10, 11 and 12, free PTX induced a dose-dependent increase of cytotoxicity in all the glioblastoma cell lines; PTX-loaded SLN followed a similar trend and showed – at the same concentration – higher efficacy than the free drug. Also the toxicity on hCMEC/D3 cells increased dose-dependently, without significant differences between free PTX and PTX-loaded SLN (Figure 13).

By comparing the cytotoxicity profile on glioblastoma cells and hCMEC/D3 cells, we can state that PTX-loaded SLN achieves significant toxicity against tumor cells at concentrations that are not toxic for BBB cells. To obtain the same degree of cytotoxicity on glioblastoma cells, free PTX

28

665 should be used at concentration that are unacceptably toxic for brain microvascular endothelial

666 cells. The different efficacy of free versus SLN-loaded PTX can be explained by the increased

667 permeability of the latter through the BBB monolayer. PTX is a known substrate of P-glycoprotein

668 (Pgp) [50], which is abundant on the luminal side of BBB cells [51]; therefore, it is a poorly

669 delivered drug into the brain parenchima. Its loading within SLN may represent a valid strategy to

670 overcome the efflux by Pgp at BBB levels.

671 In addition, also glioblastoma has been reported to be rich of Pgp [52] and multidrug resistance

672 related protein 1 (MRP1) [53], a second protein that actively effluxes PTX [50], limiting its

673 intracellular accumulation and toxicity. Therefore, a lower accumulation and toxicity of paclitaxel is

674 expected within glioblastoma cells. The loading within SLN may promote a faster uptake and/or a

675 lower efflux by Pgp and MRP1 from glioblastoma cells as well. Therefore, the loading in SLN may

676 represent a valid strategy to simultaneously bypass the drug efflux at BBB and glioblastoma levels.

4. Conclusion

The fatty acid coacervation technique, a solvent free method, was used to prepare PTX-loaded SLN.

The use of positive-charged molecules, such as ST and GCS, allowed to obtain positive SLN with sizes in the 300-600 nm range and PTX EE% in the 25-90% range.

Permeability studies through hCMEC/D3 cells monolayer, assumed as *in vitro* model of the BBB, showed a significantly increase in the permeation of Cou-6, used as model drug, when vehicled in SLN; no significantly differences in the permeability of uncharged SLN versus positively charged SLN were noted after 24 h.

Cytotoxicity studies on NO3 glioblastoma cell line demonstrated the absence of toxicity of unloaded SLN 2 and 9 and the preservation of cytotoxic activity of PTX-loaded SLN that remained always equal or greater compared with free drug.

In co-culture experiments with hCMEC/D3 and different glioblastoma cells, it was demonstrated that, when delivered in SLN, PTX increased its cytotoxicity towards glioblastoma cells, because of its increased permeation through the endothelial cell monolayer.

According to these *in vitro* results, the positive charge did not seem essential to enhance PTX brain uptake but fundamental seem to be the PTX encapsulation into SLN.

Further i.v. administration of PTX-loaded SLN in rats are in progress to confirm the suitability of SLN in enhancing PTX overcoming of the BBB.

References

[1] M.K. Nicholas, R.V. Lukas, S. Chmura, B. Yamini, M. Lesniak, P. Pytel, Molecular heterogeneity in glioblastoma: therapeutic opportunities and challenges, Semin. Oncol. 38 (2011) 243–253.

[2] M. Weller, Novel diagnostic and therapeutic approaches to malignant glioma, Swiss Med. Wkly. 141 (2011) doi:10.4414/smw.2011.13210

[3] W. Loscher, H. Potschka, Drug resistance in brain diseases and the role of drug efflux transporters, Nat. Rev. Neurosci., 6 (2005), 591-602.

[4] B.T. Hawkins, T.P. Davis, The blood-brain barrier/neurovascular unit in health and disease, Pharmacol. Rev. 57 (2005), 173-185.

[5] N.R. Saunders, C.J. Ek, M.D. Habgood, K.M. Dziegielewska, Barriers in the brain: a renaissance?, Trends Neurosci. 31 (2008), 279-286.

[6] M.L. Pinzón-Daza, I. Campia, J. Kopecka, R. Garzón, D. Ghigo, C. Riganti. Nanoparticle- and liposome-carried drugs: new strategies for active targeting and drug delivery across blood-brain barrier, Curr. Drug Metab. 14 (2013), 625-640.

[7] M.W. Brightman, T.S. Reese, Junctions between intimately apposed cell membranes in the vertebrate brain, J. Cell. Biol. 40 (1969) 648–677.

[8] A. Béduneau, P. Saulnier, J. Benoit, Active targeting of brain tumors using nanocarriers, Biomaterials 28 (2007) 4947–4967.

[9] M.S. Lesniak, U. Upadhyay, R. Goodwin, B. Tyler, H. Brem, Local delivery of doxorubicin for the treatment of malignant brain tumors in rats, Anticancer Res. 25 (2005) 3825–3831.

[10] T.F. Cloughesy, K.L. Black, Pharmacological blood–brain barrier modification for selective drug delivery, J. Neuro-Oncol. 26 (1995) 125–132.

[11] A.A. Sinkula, S.H. Yalkowsky, Rationale for design of biologically reversible drug derivatives: prodrugs, J. Pharm. Sci. 64 (1975) 181–210.

725 [12] E. Garcia-Garcia, K. Andrieux, S. Gil, P. Couvreur, Colloidal carriers and blood–brain barrier

726 (BBB) translocation: A way to deliver drugs to the brain? Int. J. Pharm. 298 (2005) 274–292.

727 [13] M.I. Alam, S. Beg, A. Samad, S. Baboota, K. Kohli, J. Ali, A. Ahuja, M. Akbar, Strategy for

728 effective brain drug delivery, Eur. J. Pharm. Sci. 40 (2010) 385–403.

729 [14] J. Kreuter, Nanoparticulate systems for brain delivery of drugs, Adv Drug Deliver Rev 47,

730 (2001) 65-81.

731 [15] P.R. Lockman, J.M. Koziara, R.J. Mumper, D.D. Allen, Nanoparticle surface charges alter

732 blood–brain barrier integrity and permeability, J. Drug Target. 12 (2004) 635–641.

733 [16] K. Park, Transport across the blood–brain barrier using albumin nanoparticles, J. Control.

734 Release 137 (2009) 1.

735 [17] A. Mistrya, S. Stolnika, L. Illum, Nanoparticles for direct nose-to-brain delivery of drugs, Int.

736 J. Pharm. 379 (2009) 146–157.

737 [18] J. Kreuter, P. Ramge, V. Petrov, S. Hamm, S.E. Gelperina, B. Engelhardt, R. Alyautdin, H.

738 Von Briesen, D.J. Begley, Direct evidence that polysorbate-80-coated poly(butylcyanoacrylate)

739 nanoparticles deliver drugs to the CNS via specific mechanisms requiring prior binding of drug to

740 the nanoparticles, Pharm. Res. 20 (2003) 409–416.

741 [19] A.E. Gulyaev, S.E. Gelperina, I.N. Skidan, A.S. Antropov, G.Y. Kivman, J. Kreuter,

742 Significant transport of doxorubicin into the brain with polysorbate 80-coated nanoparticles, Pharm.

743 Res. 16 (1999) 1564–1569.

744 [20] J. Kreuter, R.N. Alyautdin, D.A. Kharkevich, A.A. Ivanov, Passage of peptides through the

745 blood–brain barrier with colloidal polymer particles (nanoparticles), Brain Res. 674 (1995) 171–

746 174.

747 [21] S.S. Feng, L. Mu, K.Y. Win, G. Huang, Nanoparticles of biodegradable polymers for clinical

748 administration of paclitaxel, Curr. Med. Chem. 11 (2004), 413–424.

749   [22] J.M. Koziara, P.R. Lockman, D.D. Allen, R.J. Mumper, Paclitaxel nanoparticles for the

750   potential treatment of brain tumors, J. Control. Release 99 (2004) 259–269.

751   [23] J.F. Poduslo, G.L. Curran, Polyamine modification increases the permeability of proteins at the

752   blood–nerve and blood–brain barriers, J. Neurochem. 66 (1996) 1599–1609.

753   [24] Z. Nagy, H. Peters, I. Huttner, Charge-related alterations of the cerebral endothelium, Lab.

754   Invest. 49 (1983) 662–671.

755   [25] J.E. Hardebo, J. Kahrstrom, Endothelial negative surface charge areas and blood–brain barrier

756   function, Acta Physiol. Scand. 125 (1985) 495–499.

757   [26] L. Fenart, A. Casanova, B. Dehouck, C. Duhem, S. Slupek, R. Cecchelli, D. Betbeder,

758   Evaluation of effect of charge and lipid coating on ability of 60-nm nanoparticles to cross an in

759   vitro model of the blood–brain barrier, J. Pharmacol. Exp. Ther. 291 (1999) 1017–1022.

760   [27] W. Lu, Y. Zhang, Y. Tan, K. Hu, X. Jiang, S. Fu, Cationic albumin-conjugated pegylated

761   nanoparticles as novel drug carrier for brain delivery, J. Control. Release 107 (2005) 428–448.

762   [28] P. Blasi, A. Schoubben, G. Traina, G. Manfroni, L. Barberini, P.F. Alberti, C. Cirotto, M.

763   Ricci, Lipid nanoparticles for brain targeting III. Long-term stability and in vivo toxicity, Int. J.

764   Pharm. 454 (2013) 316–323.

765   [29] M. Patel, E.B. Souto, K.K. Singh, Advances in brain drug targeting and delivery: limitations

766   and challenges of solid lipid nanoparticles, Expert Opin. Drug Deliv. 10 (2013) 889-905.

767   [30] M.J. Glantz, M.C. Chamberlain, S.M. Chang, M.D. Prados, B.F. Cole, The role of paclitaxel in

768   the treatment of primary and metastatic brain tumors, Semin. Radiat. Oncol. 9 (1999) 27–33.

769   [31] S.H. Tseng, M.S. Bobola, M.S. Berger, J.R. Silber, Characterization of paclitaxel (Taxol)

770   sensitivity in human glioma- and medulloblastoma-derived cell lines, Neuro-Oncology 1 (1999)

771   101–108.

772   [32] A. Desai, T. Vyas, M. Amiji, Cytotoxicity and apoptosis enhancement in brain tumor cells

773   upon coadministration of paclitaxel and ceramide in nanoemulsion formulations, J. Pharm. Sci. 97

774   (2008) 2745–2756.

775   [33] S. Fellner, B. Bauer, D.S. Miller, M. Schaffrik, M. Fankhaenel, T. Spruh, G. Bernhardt, C.

776   Graeff, L. Faerber, H. Gschaidmeier, A. Buschsuer, G. Fricker, Transport of Paclitaxel (Taxol)

777   across the blood–brain barrier in vitro and in vivo, J. Clin. Invest. 10 (2002) 1309–1317.

778   [34] P. Ma, R.J. Mumper, Paclitaxel Nano-Delivery Systems: A Comprehensive Review, J

779   Nanomed Nanotechol 4 (2013) doi:10.4172/2157-7439.1000164

780   [35] L. Battaglia, M. Gallarate, R. Cavalli, M. Trotta, Solid lipid nanoparticles produced through a

781   coacervation method, J. Microencapsul. 27 (2010) 78–85.

782   [36] A. Trapani, J. Sitterberg, U. Bakowsky, T. Kissel, The potential of glycol chitosan

783   nanoparticles as carrier for low water soluble drugs, Int. J. Pharm. 375 (2009) 97–106.

784   [37] S. Mao, W. Sun, T. Kissel, Chitosan-based formulations for delivery of si-RNA and DNA

785   systems for protein therapeutics and antigens, Adv. Drug Del. Rev. 62 (2010) 12–27.

786   [38] B.B. Weksler, E.A. Subileau, N. Perrière, P. Charneau, K. Holloway, M. Leveque, H. Tricoire-

787   Leignel, A. Nicotra, S. Bourdoulous, P. Turowski, D.K. Male, F. Roux, J. Greenwood, I.A.

788   Romero, P.O. Couraud, Blood-brain barrier-specific properties of a human adult brain endothelial

789   cell line, Faseb. J. 19 (2005) 1872-1874.

790   [39] C. Riganti, I.C. Salaroglio, M.L. Pinzòn-Daza, V. Caldera, I. Campia, J. Kopecka, M. Mellai,

791   L. Annovazzi, P.O. Couraud, A. Bosia, D. Ghigo, D. Schiffer, Temozolomide down-regulates P-

792   glycoprotein in human blood-brain barrier cells by disrupting Wnt3-signalling, Cell Mol Life Sci

793   71 (2014) 499-516.

794   [40] V. Caldera, M. Mellai, L. Annovazzi, A. Piazzi, M. Lanotte, P. Cassoni, D. Schiffer, Antigenic

795   and Genotypic Similarity between Primary Glioblastomas and Their Derived Neurospheres, J.

796   Oncol. ID 314962 (2011) doi:10.1155/2011/314962.

797 [41] M. Trotta, E. Peira, M.E. Carlotti, M. Gallarate, Deformable liposomes for dermal

798 administration of methotrexate, Int. J. Pharm. 270, (2004) 119-125.

799 [42] L. Battaglia, M. Gallarate, E. Peira, D. Chirio, E. Muntoni, E. Biasibetti, M.T. Capucchio, A.

800 Valazza, P.P. Panciani, M. Lanotte, D. Schiffer, L. Annovazzi, V. Caldera, M. Mellai, C. Riganti,

801 Solid lipid nanoparticles for potential doxorubicin delivery in glioblastoma treatment: preliminary

802 i*n vitro* studies, J. Pharm. Sci. (2014) doi:10.1002/jps.24002.

803 [43] T.R. Mosmann, Rapid colorimetric assay for cellular growth and survival: application to

804 proliferation and cytotoxicity assay, J. Immunol. Methods 65 (1983) 55–63.

805 [44] D. Pandita, A. Ahuja, V. Lather, T. Dutta, T. Velpandian, R.K. Khar, Development,

806 characterization and *in vitro* assessement of strearylamine-based lipid nanoparticles of paclitaxel.

807 *Pharmazie* 66 (2010) 171-177.

808 [45] D. Chirio, M. Gallarate, E. Peira, L. Battaglia, L. Serpe, M. Trotta, Formulation of curcumin-

809 loaded solid lipid nanoparticles produced by fatty acids coacervation technique, J. Microencapsul.

810 28 (2011) 537-548.

811 [46] R. Asasutjarit, S. Lorenzen, S. Sirivichayakul, K. Ruxrungtham, U. Ruktanonchai, G.C.

812 Ritthidej, Effect of solid lipid nanoparticles formulation compositions on their size, zeta potential

813 and potential for in vitro pHIS-HIV-hugag, Transfection. Pharm. Res. 24 (2007) 1098-1107.

814 [47] E. Bolderson, D.J. Richard, B.B. Zhou, K.K. Khanna, Recent advances in cancer therapy

815 targeting proteins involved in DNA double-strand break repair, Clin. Cancer Res. 15 (2009) 6314–

816 6320.

817 [48] B. Pardo, B. Gómez-González, A. Aguilera, DNA repair in mammalian cells: DNA double-

818 strand break repair: how to fix a broken relationship, Cell. Mol. Life Sci. 66 (2009) 1039–1056.

819 [49] T.C. Johannessen, R. Bjerkvig, B.B. Tysnes, DNA repair and cancer stem-like cells--potential

820 partners in glioma drugresistance?, Cancer Treat. Rev. 34 (2008) 558–567.

821   [50] S. Agarwal, R. Sane, R. Oberoi, J.R. Ohlfest, W.F. Elmquist, Delivery of molecularly targeted

822   therapy to malignant glioma, a disease of the whole brain, Expert Rev. Mol. Med. 13:e17 (2011)

823   doi: 10.1017/S1462399411001888.

824   [51] L.M. Tai, A.J. Loughlin, D.K. Male, I.A. Romero, P-glycoprotein and breast cancer resistance

825   protein restrict apical-to-basolateral permeability of human brain endothelium to amyloid-β, J.

826   Cereb. Blood F. Met. 29 (2009) 1079-1083.

827   [52] A. Salmaggi, A. Boiardi, M. Gelati, A. Russo, C. Calatozzolo, E. Ciusani, F.L. Sciacca, A.

828   Ottolina, E.A. Parati, C. La Porta, G. Alessandri, C. Marras, D. Croci, M. De Rossi, GBM-derived

829   tumorospheres identify a population of tumor stem-like cells with angiogenic potential and

830   enhanced multidrug resistance phenotype, Glia 54 (2006) 850–860.

831   [53] E. Nakai, K. Park, T. Yawata, T. Chihara, A. Kumazawa, H. Nakabayashi, K. Shimizu,

832   Enhanced MDR1 expression and chemoresistance of cancer stem cells derived from GBM. Cancer

833   Invest. 27 (2009) 901–908.

FIGURE CAPTIONS

Figure A.1: Anatomical structures composing the BBB. AJs: adherent junctions. TJs: tight

junctions. ABC: ATP binding cassette transporters.

Figure 1: TEM images. a) 2200X magnification; b) 8900X magnification.

Figure 2: PTX release plots from nanoparticles using the dialysis method

Figure 3: Cou-6 permeability 0.1% dilution. * $p < 0.001$

Figure 4: Effect of 72 h treatment with increasing doses (100, 500, 1400 nM) of free and 100 nM

SLN10-encapsulated PTX on NO3 NS (b–e) and NO3 AC (g–k) growth. Control cells (a, f) did not

receive any treatment. All 200x magnification.

Figure 5: Cytotoxicity of free PTX on NS (A) and AC (B) of NO3 glioma cell line at various

dosages of drug (20, 100, 500, 1400 nM) after 72 h treatment.

Figure 6: a) cell viability of NO3 NS after 24 h treatment; b) cell viability of NO3 NS after 72 h

treatment + $p < 0.05$ vs CTRL; * $p < 0.05$ PTX-SLN vs SLN; ++ $p < 0.01$ vs CTRL; ** $p < 0.01$

PTX-SLN vs SLN

Figure 7: a) cell viability of NO3 AC after 24 h treatment; b) cell viability of NO3 AC after 72 h

treatment ++ $p < 0.01$ vs CTRL; * $p < 0.05$ PTX-SLN vs SLN;

859   Figure 8: TEM of NS after treatment with SLN15 at 15000 x. (a) After 24 h treatment with

860   unloaded SLN15. (b) After 6 h treatment with 100 nM PTX-loaded SLN15 (c) After 24 h treatment

861   with 100 nM PTX-loaded SLN15 (d) Id, large vacuoles surrounded by a membrane, (e) Id,

862   autophagolysosomes, 15000 x. (f) Possible remnants of SLN (20000 x).

863

864   Figure 9: Expression by IF of checkpoint/repair proteins in NO3 glioma cells after 72 h treatment

865   with 100 nM PTX-loaded SLN10: p-ATM, 200x (a), γ-H2AX, 200x (b), p-Chk2, 200x (c), p-

866   53BP1, 200x (d), DNA-PKcs, 200x (e), Ku70/80, 200x (f), RAD51, 200x (g) in NS; AC arrested in

867   metaphases, DAPI, 200x (j); p-ATM, 200x (k), γ-H2AX foci, 400x (i), p-Chk2, 200x (l), p-53BP1,

868   200x (m), DNA-PKcs, 200x (n), RAD51, 200x (o) in AC; nuclei counterstained with DAPI.

869   Negative reaction for p-ATM in untreated NS and AC, respectively (upper and lower left inserts of

870   panels a and i) and in NS and AC treated with unloaded SLN for 72 h (h and p); nuclei

871   counterstained DAPI, 200x.

872

873   Figure 10: cytotoxicity against CV17 cells. + $p < 0.05$ vs CTRL; ++ $p < 0.02$ vs CTRL;

874   +++ $p < 0.01$ vs CTRL; ++++ $p < 0.005$ vs CTRL; +++++ $p < 0.001$ vs CTRL; * $p < 0.05$ SLN vs

875   PTX; ** $p < 0.02$ SLN vs PTX; *** $p < 0.001$ SLN vs PTX.

876

877   Figure 11: cytotoxicity against O625 cells. + $p < 0.05$ vs CTRL; ++ $p < 0.02$ vs CTRL; +++ $p <$

878   0.01 vs CTRL; ++++ $p < 0.005$ vs CTRL; +++++ $p < 0.001$ vs CTRL; * $p < 0.05$ SLN vs PTX.

879

880   Figure 12: cytotoxicity against U87 cells. + $p < 0.01$ vs CTRL; ++ $p < 0.002$ vs CTRL; +++ $p <$

881   0.005 vs CTRL; * $p < 0.05$ SLN vs PTX; ** $p < 0.02$ SLN vs PTX; *** $p < 0.001$ SLN vs PTX.

882

883   Figure 13: cytotoxicity against hCMEC/D3 cells. + $p < 0.01$ vs CTRL; ++ $p < 0.005$ vs CTRL

884   * $p < 0.05$ SLN vs PTX; ** $p < 0.002$ SLN vs PTX.

SLN	Na-BA* (mg)	PVA 9000 (mg)	PTX (mg)	CHOL (mg)	ST (mg)	GCS (mg)	Mean diameter (nm) (PDI)	Zeta Potential (mV)
0	53	37.5	3	-	-	-	299.2 ± 0.3 (0.053)	- 3.04 ± 0.56
1	53	37.5	3	0.5	-	-	381.3 ± 20.4 (0.152)	- 3.30 ± 0.47
2	53	37.5	4.5	0.5	-	-	386.4 ± 12.3 (0.167)	- 3.34 ± 0.79
3	53	37.5	6	0.5	-	-	383.8 ± 23.2 (0.085)	- 3.41 ± 0.60
4	53	37.5	3	-	3	-	345.6 ± 9.7 (0.089)	7.85 ± 0.91
5	53	37.5	3	-	6	-	537.7 ± 13.5 (0.105)	14.37 ± 1.52
6	53	37.5	3	0.5	3	-	581.0 ± 61.1 (0.201)	8.03 ± 0.70
7	53	25	3	0.5	3	-	507.0 ± 10.5 (0.099)	10.19 ± 0.69
8	53	37.5	3	0.75	3	-	579.6 ± 7.7 (0.115)	10.40 ± 1.14
9	53	37.5	4.5	0.5	3	-	548.6 ± 20.2 (0.130)	9.07 ± 2.45
10	53	37.5	6	0.5	3		984.9 ± 93.6 (0.103)	7.65 ± 0.85
11	53	37.5	6	-	-	10	553.5 ± 5.7 (0.196)	16.90 ± 4.13
12	53	37.5	6	-	-	16	488.4 ± 19.3 (0.213)	23.79 ± 1.81
13	53	50	6	-	-	10	469.6 ± 3.8 (0.202)	15.46 ± 2.32
14	53	100	6	-	-	10	624.3 ± 16.1 (0.205)	15.64 ± 3.12
15	53	37.5	4.5	0.5	-	10	462.7 ± 32.3 (0.227)	18.21 ± 1.67
16	53	37.5	6	0.5	-	10	476.4 ± 8.4 (0.196)	20.28 ± 1.10
17	53	50	6	0.5	-	10	374.5 ± 4.8 (0.232)	19.56 ± 1.73

886

887   Table 1

888

SLN	PTX EE%	PTX LOADING (µg PTX/mg BA)
0	78 ± 4	47 ± 2
1	85 ± 5	50 ± 3
2	89 ± 3	80 ± 3
3	90 ± 3	108 ± 4
4	70 ± 6	42 ± 4
5	25 ± 3	16 ± 2
6	87 ± 4	52 ± 2
7	98 ± 2	60 ± 1
8	65 ± 6	40 ± 4
9	92 ± 4	82 ± 3
11	77 ± 2	92 ± 2
12	81 ± 4	98 ± 5
13	52 ± 5	62 ± 6
14	24 ± 3	28 ± 3
15	83 ± 4	74 ± 3
16	83 ± 3	100 ± 4
17	75 ± 5	90 ± 6

889

890   Table 2

891

		SLN 9	SLN 15	SLN 16	SLN 17
7 days	Size (nm)	682.4 ± 15.1	783.2 ± 74.3	554.2 ± 9.5	500.1 ± 6.4
	%EE	92 ± 3	81 ± 2	80 ± 2	74 ± 3
	Zeta potential (mV)	9.15 ± 0.85	13.4 ± 0.9	15.9 ± 2.8	18.3 ± 1.6
30 days	Size (nm)	1500.0 ± 21.6	799.7 ± 63.2	598.1 ± 14.6	599.2 ± 9.5
	%EE	91 ± 4	80 ± 3	79 ± 3	73 ± 2
	Zeta potential (mV)	9.05 ± 0.54	11.6 ± 1.4	14.5 ± 3.3	14.4 ± 3.1
60 days	Size (nm)	1536.8 ± 39.2	933.8 ± 17.9	669.8 ± 27.3	686.1 ± 12.4
	%EE	89 ± 4	80 ± 3	71 ± 2	73 ± 2
	Zeta potential (mV)	9.07 ± 0.65	10.7 ± 2.1	13.9 ± 3.4	12.9 ± 4.1

892

893   Table 3

894

	SLN 9	SLN 15	SLN 16	SLN 17
Mean diameter (nm)	842.0 ± 17.9	632.4 ± 18.4	592.3 ± 18.0	408.4 ± 5.8
Zeta potential (mV)	8.66 ± 1.02	18.56 ± 1.34	19.68 ± 1.98	19.87 ± 1.45
PTX EE%	88 ± 3	81 ± 2	83 ± 2	89 ± 3

895   Table 4

896
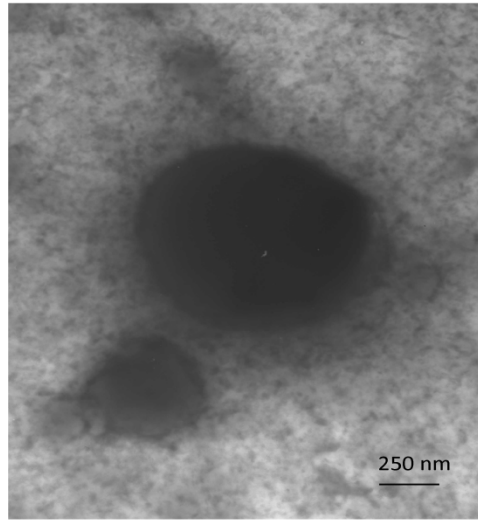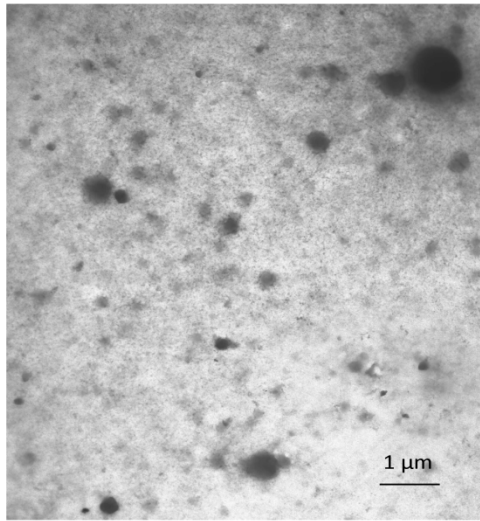
Figure 1a and 1b

Chirio et al

897

898

899
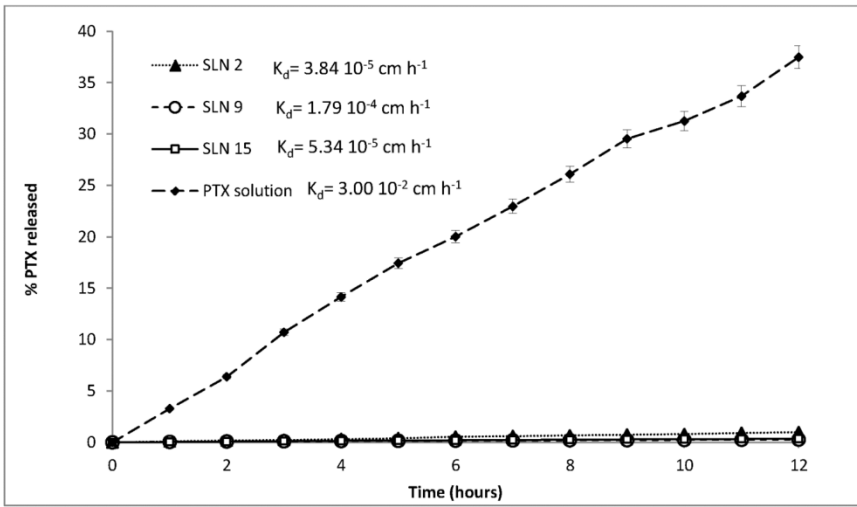
Figure 2

Chirio et al

900

901

902
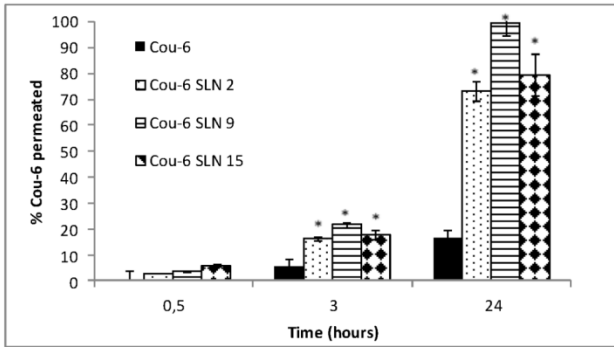
Figure 3

Chirio et al

903

904
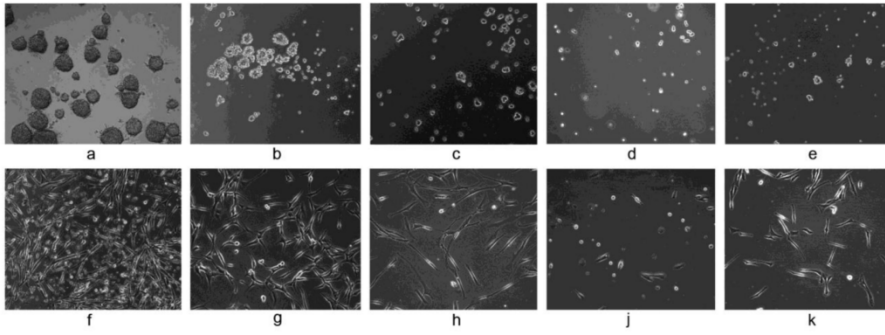
Figure 4

Chirio et al

905

906
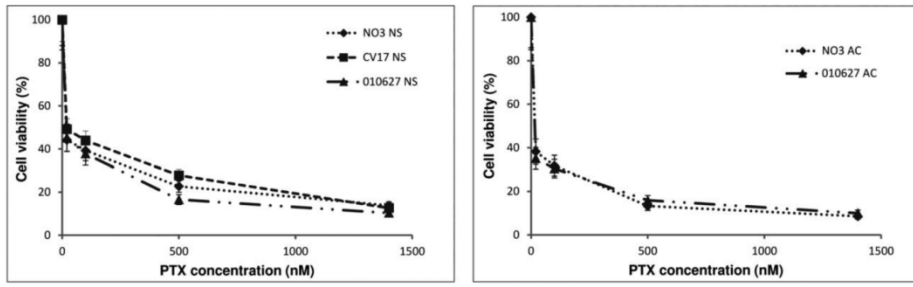
Figure 5

Chirio et al

907

908
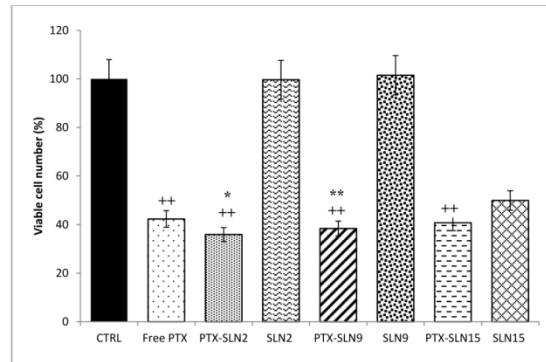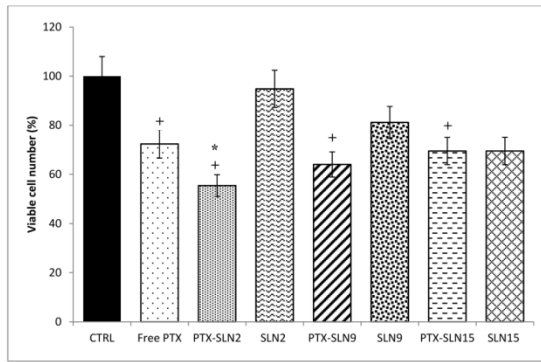
Figure 6

Chirio et al

909

910
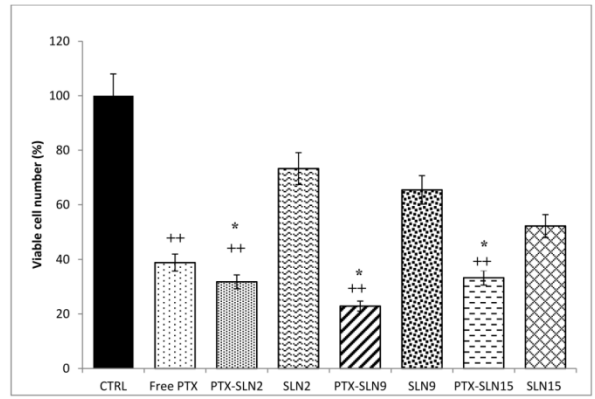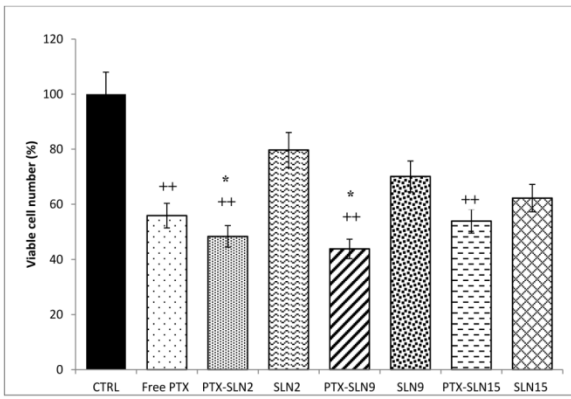
Figure 7

Chirio et al

911

912
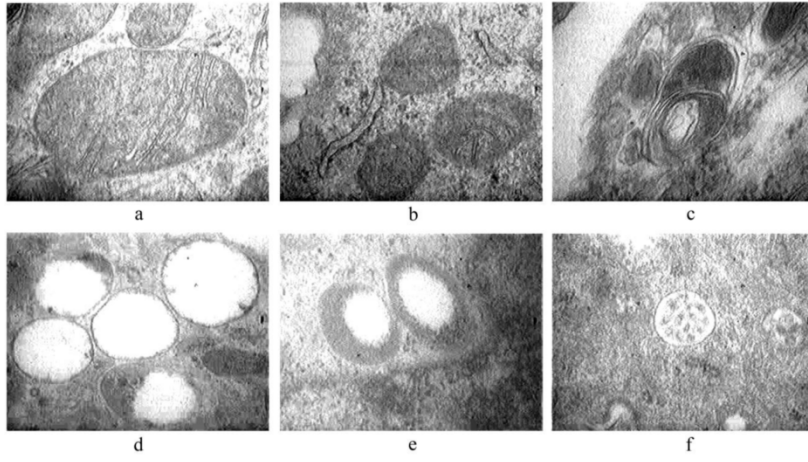
Figure 8

Chirio et al
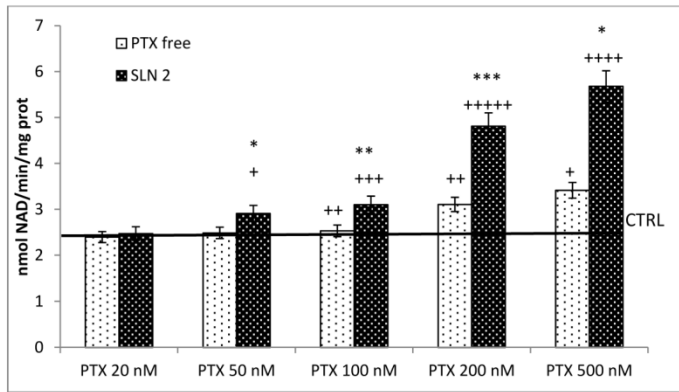
913

914
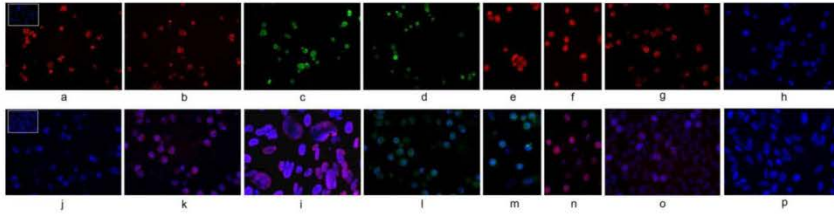
Figure 9

Chirio et al
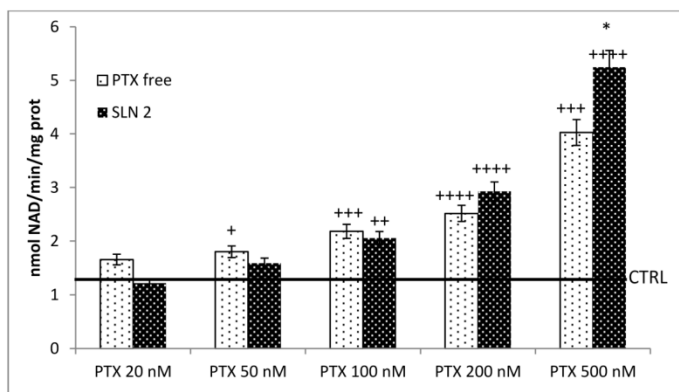
915

916

Figure 10

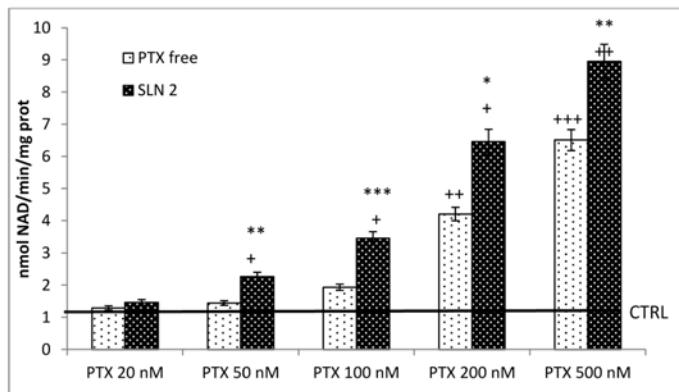Chirio et al

917

918

Figure 11

Chirio et al

919

920

Figure 12

Chirio et al

921

922

Figure 13

Chirio et al

923